

Possible Fano effect and suppression of Andreev reflection in $\text{La}_3\text{Ni}_2\text{O}_7$

Yi-feng Yang^{1,2,3,*}

¹Beijing National Laboratory for Condensed Matter Physics and Institute of Physics,
Chinese Academy of Sciences, Beijing 100190, China

²University of Chinese Academy of Sciences, Beijing 100049, China

³Songshan Lake Materials Laboratory, Dongguan, Guangdong 523808, China

(Dated: August 27, 2024)

The recently-discovered high-temperature superconductor $\text{La}_3\text{Ni}_2\text{O}_7$ under high pressure has stimulated intensive debates. Key controversies concern interlayer versus intralayer pairing scenarios and if the hybridization plays a key role in establishing the superconductivity. But experimental clarification is difficult due to the limitation of employing state-of-the-art techniques under high pressure. Here we propose that quasiparticle tunneling and Andreev reflection on a normal metal-superconductor junction may provide a feasible way to distinguish different pairing scenarios. We predict that an asymmetric Fano line shape may be induced by the hybridization between the $d_{x^2-y^2}$ metallic bands and the strongly renormalized flat d_{z^2} quasiparticle bands. In the superconducting state, we show that the Andreev reflection should be greatly suppressed for interlayer pairing superconductivity with a small interlayer hopping. We propose future experiments to examine these predictions and help clarify the fundamental physics of superconducting $\text{La}_3\text{Ni}_2\text{O}_7$.

The recent discovery of high-temperature superconductivity in the bilayer nickelate $\text{La}_3\text{Ni}_2\text{O}_7$ under high pressure has stimulated intensive theoretical debates concerning its electronic band structures and potential pairing mechanism [1–3]. Although experiments at ambient pressure have helped to clarify many important issues [4–14], direct probes of its superconducting properties are very challenging due to the high pressure. One of the fundamental issues involves the nature of its pairing mechanism. While many propose interlayer pairing mediated by the interlayer superexchange interaction of d_{z^2} orbitals [15–29], some argue that the superconductivity is similar to that in cuprates [30–32]. Among all interlayer pairing scenarios, debates also exist concerning the role of the Hund’s rule coupling and the hybridization between the $d_{x^2-y^2}$ and d_{z^2} orbitals [17, 24, 33]. In the two-component scenario, it is the hybridization that helps mobilize the local d_{z^2} interlayer pairs and induces the long-range phase coherence [15, 17]. While in the Hund scenario, the hybridization and the self-doping to the d_{z^2} orbitals are both harmful, and it is the Hund’s rule coupling that transfers the interlayer superexchange interaction between localized d_{z^2} orbitals to the itinerant $d_{x^2-y^2}$ orbitals to form interlayer Cooper pairing [24]. It is therefore important to distinguish the intralayer and interlayer pairing mechanisms and provide experimental evidences for the presence of the hybridization.

However, high pressure has prevented the application of many important techniques. Among the very few exceptions, quasiparticle tunneling and Andreev reflection may be a feasible way to provide some useful microscopic information on the electronic and superconducting properties. In this work, we argue that they might indeed exhibit distinct properties and help distinguish different pairing scenarios in superconducting $\text{La}_3\text{Ni}_2\text{O}_7$. In particular, we show the possibility of Fano effect in the quasi-

particle tunneling spectra if hybridization indeed exists between the broad $d_{x^2-y^2}$ metallic bands and the strongly renormalized flat d_{z^2} quasiparticle bands, and that, in contrast to intralayer pairing superconductivity, the Andreev reflection may be greatly suppressed for interlayer pairing with small interlayer hopping. We suggest future experiments to verify these predictions.

The total Hamiltonian of a normal metal-superconductor junction contains three parts:

$$H = H_s + H_m + H_c, \quad (1)$$

where H_s , H_m , and H_c describe the nickelate superconductor, the normal metal lead, and their coupling term, respectively. The $\text{La}_3\text{Ni}_2\text{O}_7$ Hamiltonian takes an effective two-orbital bilayer form [15, 17, 29]:

$$H_s = \sum_{l\mathbf{a}\mathbf{k}s} \epsilon_{\mathbf{k}}^a d_{l\mathbf{a}\mathbf{k}s}^\dagger d_{l\mathbf{a}\mathbf{k}s} - \sum_{l\mathbf{k}s} V_{\mathbf{k}} \left(d_{l1\mathbf{k}s}^\dagger d_{l2\mathbf{k}s} + h.c. \right) - t_{\perp} \sum_{\mathbf{k}s} \left(d_{11\mathbf{k}s}^\dagger d_{21\mathbf{k}s} + h.c. \right) + J \sum_i \mathbf{S}_{1i} \cdot \mathbf{S}_{2i}, \quad (2)$$

where $d_{l\mathbf{a}\mathbf{k}\sigma}^\dagger$ creates one d_{z^2} ($a = 1$) or $d_{x^2-y^2}$ ($a = 2$) electron of spin s and momentum \mathbf{k} on l -th layer ($l = 1, 2$) $\mathbf{S}_{li} = \frac{1}{2} \sum_{ss'} d_{l1is}^\dagger \boldsymbol{\sigma}_{ss'} d_{l1is}$ is the d_{z^2} spin density operator on site i of l -th layer with $\boldsymbol{\sigma}$ being the Pauli matrices, $\epsilon_{\mathbf{k}}^a$ gives the dispersion of a -th orbital within each layer, $V_{\mathbf{k}}$ is the intralayer nearest-neighbor hybridization between two orbitals, t_{\perp} is the interlayer hopping of d_{z^2} quasiparticles, and J is their interlayer superexchange interaction mediated by the apical oxygens. First-principles calculations give $\epsilon_{\mathbf{k}}^a = -2t_a(\cos \mathbf{k}_x + \cos \mathbf{k}_y) + 4t'_a \cos \mathbf{k}_x \cos \mathbf{k}_y + \epsilon_0^a$ and $V_{\mathbf{k}} = -2V(\cos \mathbf{k}_x - \cos \mathbf{k}_y)$, where $t_1 = 0.11$, $t'_1 = -0.017$, $\epsilon_0^1 = 0.409$, $t_2 = 0.483$, $t'_2 = 0.069$, $\epsilon_0^2 = 0.776$, $V = 0.239$, and $t_{\perp} = 0.635$ [34]. For simplicity, we drop the energy unit eV throughout this paper unless noted. Other small parameters are

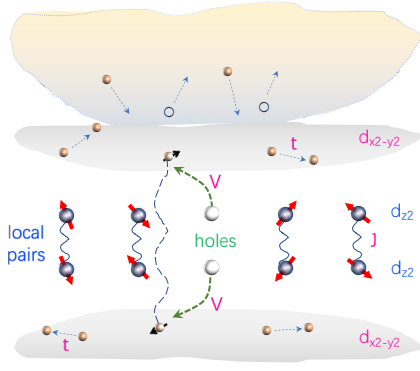


FIG. 1: Illustration of the the normal metal/interlayer pairing superconductor junction and the effective t - V - J model for the bilayer nickelate, where t is the hopping parameter of the metallic band, J is the interlayer superexchange interaction of the local pairing orbital, and V is their hybridization. The electrons may tunnel into both the broad $d_{x^2-y^2}$ bands and the relatively narrow d_{z^2} bands in the top layer. The Fano interference arises because of the hybridization of the two bands. The Andreev reflection may be reduced when $t_{\perp} \rightarrow 0$ because of the interlayer pairing mechanism.

ignored for simplicity and their effects may be partly included by renormalizing the above tight-binding parameters [17, 35]. The intralayer superexchange interaction is also ignored to focus only on the interlayer pairing since it is ten times smaller than the interlayer superexchange J as estimated lately in the resonant inelastic X-ray scattering (RIXS) and inelastic neutron scattering (INS) measurements [9, 10]. The lead and their coupling term can be described as

$$H_m = \sum_{\mathbf{k}s} \xi_{\mathbf{k}} c_{\mathbf{k}s}^{\dagger} c_{\mathbf{k}s}, \quad H_c = \sum_{a\mathbf{k}s} t_{\mathbf{k}}^a c_{\mathbf{k}s}^{\dagger} d_{1a\mathbf{k}s}, \quad (3)$$

where $\xi_{\mathbf{k}}$ is the dispersion of the noninteracting electrons in the normal metal lead and $t_{\mathbf{k}}^a$ is the tunneling matrix into the a -th orbital.

Figure 1 gives a schematic illustration of the whole setup. The quasiparticle tunneling and Andreev reflection can be studied using the Keldysh Green's function technique [36]. Applying a bias voltage V_b on the lead induces a finite electric current [37–39]:

$$\begin{aligned} I &= -e \frac{dN_c}{dt} = -i \frac{e}{\hbar} \sum_{a\mathbf{k}s} t_{\mathbf{k}}^a \langle d_{1a\mathbf{k}s}^{\dagger} c_{\mathbf{k}s} \rangle + c.c. \\ &= \frac{e}{\hbar} \int d\omega [f(\omega - eV_b) - f(\omega)] T(\omega), \end{aligned} \quad (4)$$

where $N_c = \sum_{\mathbf{k}s} c_{\mathbf{k}s}^{\dagger} c_{\mathbf{k}s}$ is the total number of electrons in the lead, $f(\omega)$ is the Fermi distribution function, and we have the scattering matrix:

$$T(\omega) = \sum_{aa'a''\mathbf{k}s} \Gamma_{\mathbf{k}}^0 \Gamma_{\mathbf{k}}^{aa'} \mathcal{G}_{a'\mathbf{k}s, a''\mathbf{k}s}^R(\omega) \mathcal{G}_{a''\mathbf{k}s, a\mathbf{k}s}^A(\omega), \quad (5)$$

where $\Gamma_{\mathbf{k}}^0$ measures the quasiparticle line width in the top NiO layer, $\Gamma_{\mathbf{k}}^{aa'} = 2\pi t_{\mathbf{k}}^a t_{\mathbf{k}}^{a'} \rho_{\mathbf{k}}^c(\omega)$ with $\rho_{\mathbf{k}}^c(\omega)$ being

the spectral function of the lead electrons, and $\mathcal{G}^{R/A}$ denote the retarded/advanced Green's functions of the top layer ($l = 1$) in the Nambu representation $\psi_{\mathbf{k}}^{\dagger} = (d_{11\mathbf{k}\uparrow}^{\dagger}, d_{12\mathbf{k}\uparrow}^{\dagger}, d_{11\mathbf{k}\downarrow}, d_{12\mathbf{k}\downarrow})$. The total scattering can thus be split into two terms, $T(\omega) = T^Q(\omega) + T^A(\omega)$, where T^Q and T^A describe the quasiparticle tunneling and Andreev reflection contributions, respectively. We have

$$\begin{aligned} T^Q(\omega) &= \sum_{aa'a''\mathbf{k}s} \Gamma_{\mathbf{k}}^0 \Gamma_{\mathbf{k}}^{aa'} G_{a'\mathbf{k}s, a''\mathbf{k}s}^R(\omega) G_{a''\mathbf{k}s, a\mathbf{k}s}^A(\omega), \\ T^A(\omega) &= \sum_{aa'a''\mathbf{k}s} \Gamma_{\mathbf{k}}^0 \Gamma_{\mathbf{k}}^{aa'} F_{a'\mathbf{k}s, a''\mathbf{k}\bar{s}}^R(\omega) F_{a''\mathbf{k}\bar{s}, a\mathbf{k}s}^{\dagger, A}(\omega), \end{aligned} \quad (6)$$

where $G^{R/A}$ and $F^{R/A}$ are the normal and anomalous components of the Green's function $\mathcal{G}^{R/A}$ in the Nambu representation, respectively. In the following, we will discuss T^Q and T^A separately.

In the above formalism, only the Green's functions of the top layer ($l = 1$) are explicitly involved. To calculate them, we employ the mean-field approximation and decouple the superexchange term, $J \mathbf{S}_{1i} \cdot \mathbf{S}_{2i} \rightarrow \sqrt{2} (\Delta^* \Phi_i + \bar{\Phi}_i \Delta)$, where $\Phi_i = \frac{1}{\sqrt{2}} (d_{11i\downarrow} d_{21i\uparrow} - d_{11i\uparrow} d_{21i\downarrow})$ represents the local interlayer d_{z^2} pairing at site i and Δ is the static uniform pairing field. The mean-field approximation ignores the correlation effects as well as the spatial and temporal fluctuations of the superconductivity, so that all energy scales may be strongly renormalized and altered in real experiment, in particularly near the Fermi energy. Nevertheless, it still provides a reasonable starting point for studying qualitative features of the quasiparticle tunneling and Andreev reflection. Under the mean-field approximation, the Hamiltonian takes a bilinear form which can be solved straightforwardly in the momentum space.

To obtain the Green's functions, we first integrate out the electron degrees of freedom of the lead and the bottom layer ($l = 2$). Under the Nambu basis $\psi_{\mathbf{k}}$, we derive the Green's function matrix for the top layer,

$$(\mathcal{G}_{\mathbf{k}}^R)^{-1} = g_{\mathbf{k}}^{-1} I - \mathcal{H}_{\mathbf{k}}^0 - \Sigma_{\mathbf{k}} - M [g_{\mathbf{k}}^{-1} I - \mathcal{H}_{\mathbf{k}}^0]^{-1} M^{\dagger}, \quad (7)$$

where $g_{\mathbf{k}}^{-1} = \omega + i\Gamma_{\mathbf{k}}^0/2$, I is the 4×4 unit matrix, and

$$\begin{aligned} \mathcal{H}_{\mathbf{k}}^0 &= \begin{pmatrix} \epsilon_{\mathbf{k}}^1 & -V_{\mathbf{k}} & 0 & 0 \\ -V_{\mathbf{k}} & \epsilon_{\mathbf{k}}^2 & 0 & 0 \\ 0 & 0 & -\epsilon_{\mathbf{k}}^1 & V_{\mathbf{k}} \\ 0 & 0 & V_{\mathbf{k}} & -\epsilon_{\mathbf{k}}^2 \end{pmatrix}, \quad M = \begin{pmatrix} -t_{\perp} & 0 & \Delta & 0 \\ 0 & 0 & 0 & 0 \\ \Delta^* & 0 & t_{\perp} & 0 \\ 0 & 0 & 0 & 0 \end{pmatrix}, \\ \Sigma_{\mathbf{k}} &= -\frac{i}{2} \begin{pmatrix} \Gamma_{\mathbf{k}}^{11} & \Gamma_{\mathbf{k}}^{12} & 0 & 0 \\ \Gamma_{\mathbf{k}}^{21} & \Gamma_{\mathbf{k}}^{22} & 0 & 0 \\ 0 & 0 & \Gamma_{\mathbf{k}}^{11} & \Gamma_{\mathbf{k}}^{12} \\ 0 & 0 & \Gamma_{\mathbf{k}}^{21} & \Gamma_{\mathbf{k}}^{22} \end{pmatrix}. \end{aligned} \quad (8)$$

To simplify the numerical calculations, we further ignore the momentum dependence in $\Gamma_{\mathbf{k}}^0$ and $\Gamma_{\mathbf{k}}^{11}$, assume

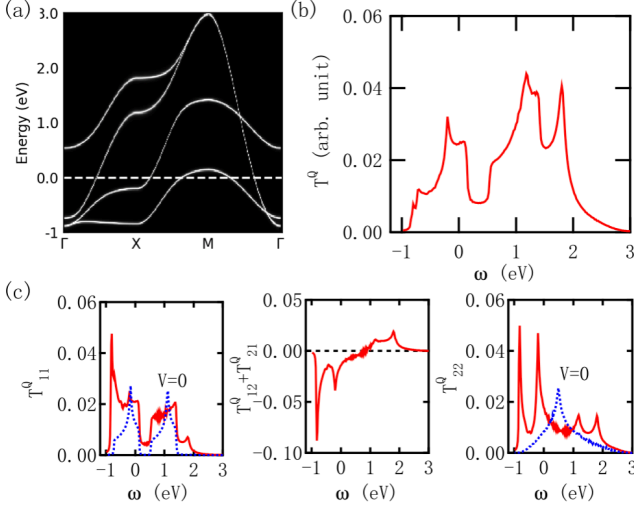


FIG. 2: (a) Spectral function calculated based on the tight-binding parameters and $\Gamma^0 = \Gamma^{aa'} = 0.01$. (b) The corresponding quasiparticle tunneling spectra showing multiple peaks. (c) Three components of the quasiparticle tunneling coefficient, showing a significant contribution from the off-diagonal term. The dotted lines show T_{11}^Q and T_{22}^Q at $V = 0$ for comparison.

$\Gamma_{\mathbf{k}}^0 \equiv \Gamma^0$, $\Gamma_{\mathbf{k}}^{11} \equiv \Gamma^{11}$, $\Gamma_{\mathbf{k}}^{12/21} = \Gamma^{12/21}(\cos \mathbf{k}_x - \cos \mathbf{k}_y)$, and $\Gamma_{\mathbf{k}}^{22} = \Gamma^{22}(\cos \mathbf{k}_x - \cos \mathbf{k}_y)^2$, and set $\Gamma^{12} = \Gamma^{21} = r\Gamma^{22}$ and $\Gamma^{11} = r^2\Gamma^{22}$. Here r is the ratio of the tunneling t^a into d_{z^2} and $d_{x^2-y^2}$ orbitals and $(\cos \mathbf{k}_x - \cos \mathbf{k}_y)$ accounts for the effect of the sign change of the $d_{x^2-y^2}$ wave function along x and y directions on $t_{\mathbf{k}}^2$ assuming the lead electrons have isotropic wave functions. We also require that Δ , Γ^0 , Γ^{22} , and r are real numbers.

To verify the above formalism, we first show in Fig. 2(a) the calculated spectral function $A_{\mathbf{k}}(\omega) = -\pi^{-1} \text{Im} \sum_{as} G_{1a\mathbf{k}s, 1a\mathbf{k}s}^R(\omega)$ along a high symmetry path for $\Gamma^0 = \Gamma^{22} = 0.01$, $r = 1$, and $\Delta = 0$ using the tight-binding parameters. Direct comparisons with previous work confirm our derived band structures, which contains both bonding (around the Fermi energy) and antibonding bands of d_{z^2} orbitals and several flat pieces induced by their hybridization with the broader $d_{x^2-y^2}$ bands [34]. Substituting the derived Green's functions in Eq. (6) gives the quasiparticle tunneling coefficient $T^Q(\omega)$. Its numerical results are plotted in Fig. 2(b) and exhibit multiple pronounced peaks corresponding to the flat pieces of the bands, which reflect the interplay between the van Hove singularities and the hybridization between the d_{z^2} and $d_{x^2-y^2}$ bands. For clarity, we also plot in Fig. 2(c) its three components, T_{11}^Q , $T_{12}^Q + T_{21}^Q$, and T_{22}^Q , where $T_{aa'}^Q = \sum_{a''\mathbf{k}s} \Gamma_{\mathbf{k}}^0 \Gamma_{\mathbf{k}}^{aa'} G_{1a'\mathbf{k}s, 1a''\mathbf{k}s}^R G_{1a''\mathbf{k}s, 1a\mathbf{k}s}^A$. There exists a substantial contribution from the interference term, $T_{12}^Q + T_{21}^Q$, in particular at negative energies where a sharp peak is almost completely cancelled out with those in T_{11}^Q and T_{22}^Q . This corresponds to the flat

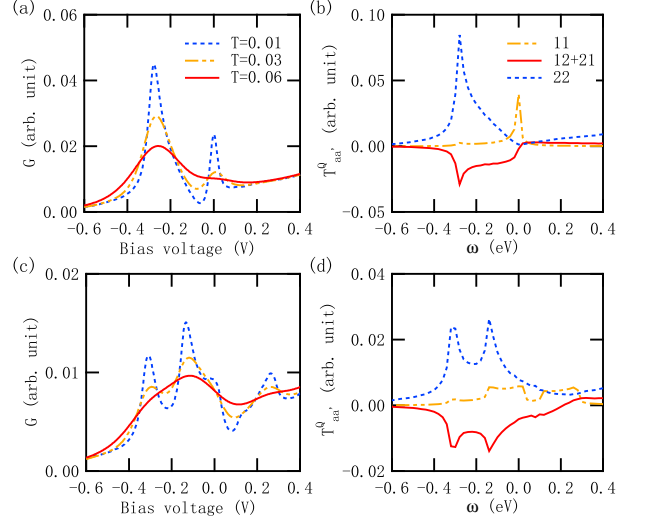


FIG. 3: (a) Differential conductance $G = dI(V_b)/dV_b$ from quasiparticle tunneling for the tight-binding parameters with $\eta_t = 0$, $\eta_V = 0.5$, $\Gamma^0 = \Gamma^{22} = 0.01$, and $r = 0.2$ for the temperature $T = 0.01, 0.03, 0.06$. (b) Three components of the corresponding quasiparticle tunneling coefficient, T_{11}^Q , $T_{12}^Q + T_{21}^Q$, and T_{22}^Q . (c) Differential conductance $G = dI/dV$ for the tight-binding parameters with $\eta_t = 0.2$, $\eta_V = 0.5$, $\Gamma^0 = \Gamma^{22} = 0.01$, and $r = 0.3$ for $T = 0.01, 0.03, 0.06$, showing additional peaks due to the bonding-antibonding splitting at low temperature but a broad asymmetric line shape at high temperature. (d) Three components of the quasiparticle tunneling coefficient, T_{11}^Q , $T_{12}^Q + T_{21}^Q$, and T_{22}^Q for (c). For simplicity, we have ignored the temperature dependence of all parameters.

band close to -1, which will be renormalized towards the Fermi energy once correlation effects are correctly taken into account. The valley between 0 and 0.5 only appears in T_{11}^Q , corresponding to the bonding-antibonding splitting region of the d_{z^2} bands, below which the low-energy physics is governed by the bonding orbitals. For comparison, the quasiparticle tunneling coefficients without hybridization ($V = 0$) are also shown in Fig. 2(c).

To have a better view of the interference effect in the low-energy region, we plot in Fig. 3 the quasiparticle tunneling coefficient in a smaller energy window around the Fermi energy and take into consideration the renormalization effect by tuning $\epsilon_{\mathbf{k}}^1 \rightarrow \eta_t \epsilon_{\mathbf{k}}^1$, $t_{\perp} \rightarrow \eta_t t_{\perp}$, and $V \rightarrow \eta_V V$, where η_t and η_V may be regarded to arise from the Gutzwiller projection for the nearly half-filled d_{z^2} orbitals in $\text{La}_3\text{Ni}_2\text{O}_7$ but are taken here as free parameters. Figure 3(a) shows the temperature evolution of the differential conductance $G(V_b) = dI(V_b)/dV_b$ as a function of the bias voltage for $\eta_t = 0$, $\eta_V = 0.5$, $\Gamma^0 = \Gamma^{22} = 0.01$, and $r = 0.2$. We have deliberately chosen the extreme case with $\eta_t = 0$ to reflect a strongly renormalized flat d_{z^2} quasiparticle bands, so that we may ignore other complications as discussed in Fig. 2 and fo-

cus only on the hybridization effect in the quasiparticle tunneling. The ratio r of the tunneling parameters into d_{z^2} and $d_{x^2-y^2}$ orbitals should be correspondingly renormalized and therefore assigned a small number, which helps to suppress the d_{z^2} quasiparticle weight ignored in the mean-field approximation. In the extreme case where d_{z^2} electrons are fully localized, possibly at ambient pressure, we should have $\eta_t = \eta_V = r = 0$ and the electrons can only tunnel into the $d_{x^2-y^2}$ orbital, giving rise to a broad background.

As is seen clearly in Fig. 3(a), the differential conductance $G(V_b)$ develops an asymmetric feature below the Fermi energy, which follows roughly a Fano-like line shape on top of the broad background from the $d_{x^2-y^2}$ metallic bands without hybridization. The suppression below $V = 0$ reflects the destructive interference from the off-diagonal term $T_{12}^Q + T_{21}^Q$, which is not present without hybridization. This is better seen in Fig. 3(b), where we plot the three components of the quasiparticle tunneling coefficient $T^Q(\omega)$. The off-diagonal term remains almost unchanged around $\omega = -0.2$, which cancels out the diagonal contribution from $T_{11}^Q(\omega)$ and $T_{22}^Q(\omega)$ and yields the conductance minimum at negative V slightly below zero bias. At low temperature, this suppression of $G(V_b)$ is interrupted by an unexpected peak at $V = 0$. This peak only appears in T_{11}^Q in Fig. 3(b) and is therefore a property solely of d_{z^2} . We attribute it to the nodal hybridization along the zone diagonal ($k_x = k_y$) direction, which leaves a finite contribution of the d_{z^2} flat bands on the Fermi energy. In any case, the Fano interference effect is clearly identified to arise from the hybridization between the strongly renormalized flat d_{z^2} quasiparticle bands and the broad metallic $d_{x^2-y^2}$ bands.

However, due to the complication of realistic electronic structures, it is not clear if the Fano effect can be easily resolved in experiment. To see this, we compare in Fig. 3(c) the differential conductance for a finite $\eta_t = 0.2$, which corresponds to narrow but dispersive d_{z^2} quasiparticle bands. Other parameters remain unchanged except for a slightly larger $r = 0.3$. At low temperatures, the $G(V_b)$ curves become very different, where the single peak near -0.3 V in Fig. 3(a) splits into two, while the peak on the Fermi energy is suppressed. These changes are not surprising and arise owing to the finite dispersion of d_{z^2} quasiparticle bands. As a result, there appear many additional peaks and the Fano feature is no longer discernible. However, at higher temperature $T = 0.03$, all peaks get broadened and an overall asymmetric line shape can still be revealed on the broad background, reflecting a signature of the hybridization-induced interference. For completeness, Fig. 3(d) compares the three components of the corresponding quasiparticle tunneling coefficient. We see an equally large but negative off-diagonal contribution for the destructive interference. On the other hand, this off-diagonal term may be overwhelmed if the coupling of the lead with the d_{z^2} orbital is

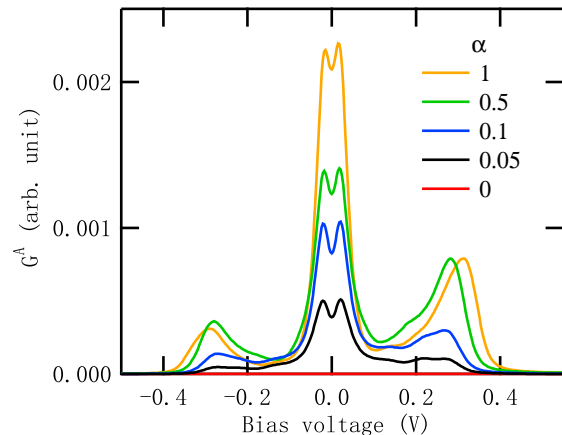


FIG. 4: (a) Different conductance contributed by the Andreev reflection coefficient using the tight-binding parameters with $\eta_t = 0.2$, $\eta_V = 0.5$, $\Gamma^0 = \Gamma^{22} = 0.01$, $r = 0.3$, and the pairing order parameter $\Delta = 0.02$ for the renormalized $t_\perp \rightarrow \alpha\eta_t t_\perp$ with varying $\alpha = 1, 0.5, 0.1, 0.05, 0$ at $T = 0.01$.

too strong (large r). This is possible considering the d_{z^2} quasiparticle wave function, though renormalized with a small spectral weight, is perpendicular to the NiO plane and may have a larger overlap with the lead electrons than that of the $d_{x^2-y^2}$ orbital. Then the differential conductance around zero bias would be governed by the features of the d_{z^2} spectra as shown in $T_{11}^Q(\omega)$. We leave for future experiment to see if the hybridization-induced Fano interference effect may be resolved in real measurements of pressurized $\text{La}_3\text{Ni}_2\text{O}_7$, which may depend on the specific parameter range in experiment. Similar Fano phenomena have been predicted and observed previously in heavy-fermion materials [40].

Now we turn to the superconducting state and study the Andreev reflection for interlayer pairing. Figure 4 shows the typical differential conductance $G^A(V_b)$ contributed solely by the Andreev reflection coefficient $T^A(\omega)$ assuming $\Delta = 0.02$ for the interlayer pairing. To study how it evolves with interlayer hopping, we further reduce $\eta_t t_\perp \rightarrow \alpha\eta_t t_\perp$ by multiplying an additional factor $\alpha = 0.5, 0.1, 0.05$, and 0 . Other parameters are the same as in Fig. 3(d). For finite α , we see clearly the Andreev reflection peak around zero energy. By contrast, one expects a V- or U-shape gap for the quasiparticle tunneling contribution. However, as α decreases, the height of the peak is gradually reduced and eventually diminishes for $\alpha = 0$. Thus, the Andreev reflection is completely suppressed without interlayer hopping, which reveals a distinct feature compared to that of intralayer pairing superconductivity. The suppression is in some sense analogous to the junction of a fully polarized ferromagnet and a spin-singlet superconductor. It is easy to understand because Andreev reflection only occurs when

incident electrons can form Cooper pairs in the superconductor and be reflected as holes, but this process is impossible for interlayer pairing superconductivity if the incident electrons can only tunnel into the top layer. A finite t_{\perp} not only induces a higher-order intralayer pairing component but also allows for the tunneling into the bottom layer, thus contributing a finite Andreev reflection coefficient. However, for small t_{\perp} that has been greatly renormalized by strong electronic correlations in nearly half-filled d_{z^2} orbitals, our results indicate a much weaker Andreev reflection compared to that of usual intralayer pairing superconductors. This is a fundamental difference that may help distinguish interlayer and intralayer pairing superconductivity.

To summarize, we propose to examine the hybridization physics and different pairing mechanisms using the normal metal-superconductor junction for $\text{La}_3\text{Ni}_2\text{O}_7$ under pressure. We show that the hybridization may lead to a Fano interference effect with an asymmetric line shape in the quasiparticle tunneling of the normal state, and the small interlayer hopping may suppress the Andreev reflection for interlayer pairing. The former may be used to establish the hybridization between the $d_{x^2-y^2}$ metallic bands and the flat d_{z^2} quasiparticle bands, and thus clarify the microscopic basis for the two-component theory of superconductivity, while the latter may help distinguish the interlayer and intralayer pairing scenarios. Given the difficulty in employing other state-of-the-art techniques under high pressure, our proposal may be a feasible way to clarify these fundamental issues in superconducting $\text{La}_3\text{Ni}_2\text{O}_7$.

This work was supported by the National Natural Science Foundation of China (Grants No. 12474136), the Strategic Priority Research Program of the Chinese Academy of Sciences (Grant No. XDB33010100), and the National Key Research and Development Program of China (Grant No. 2022YFA1402203).

* yifeng@iphy.ac.cn

- [1] H. Sun, M. Huo, X. Hu, J. Li, Z. Liu, Y. Han, L. Tang, Z. Mao, P. Yang, B. Wang, J. Cheng, D.-X. Yao, G.-M. Zhang, and M. Wang, Signatures of superconductivity near 80 K in a nickelate under high pressure, *Nature* **621**, 493 (2023).
- [2] J. Hou, P. T. Yang, Z. Y. Liu, J. Y. Li, P. F. Shan, L. Ma, G. Wang, N. N. Wang, H. Z. Guo, J. P. Sun, Y. Uwatoko, M. Wang, G.-M. Zhang, B. S. Wang, and J.-G. Cheng, Emergence of high-temperature superconducting phase in the pressurized $\text{La}_3\text{Ni}_2\text{O}_7$ crystals, *Chin. Phys. Lett.* **40**, 117302 (2023).
- [3] Y. Zhang, D. Su, Y. Huang, Z. Shan, H. Sun, M. Huo, K. Ye, J. Zhang, Z. Yang, Y. Xu, Y. Su, R. Li, M. Smidman, M. Wang, L. Jiao, and H. Yuan, High-temperature superconductivity with zero-resistance and strange-metal behaviour in $\text{La}_3\text{Ni}_2\text{O}_{7-\delta}$, *Nat. Phys.* **20**, 1269 (2024).
- [4] Z. Liu, M. Huo, J. Li, Q. Li, Y. Liu, Y. Dai, X. Zhou, J. Hao, Y. Lu, M. Wang, and H.-H. Wen, Electronic correlations and partial gap in the bilayer nickelate $\text{La}_3\text{Ni}_2\text{O}_7$, arXiv:2307.02950.
- [5] J. Yang, H. Sun, X. Hu, Y. Xie, T. Miao, H. Luo, H. Chen, B. Liang, W. Zhu, G. Qu, C.-Q. Chen, M. Huo, Y. Huang, S. Zhang, F. Zhang, F. Yang, Z. Wang, Q. Peng, H. Mao, G. Liu, Z. Xu, T. Qian, D.-X. Yao, M. Wang, L. Zhao, and X. J. Zhou, Orbital-dependent electron correlation in double-layer nickelate $\text{La}_3\text{Ni}_2\text{O}_7$, *Nat. Commun.* **15**, 4373 (2024).
- [6] K. Chen, X. Liu, J. Jiao, M. Zou, C. Jiang, X. Li, Y. Luo, Q. Wu, N. Zhang, Y. Guo, and L. Shu, Evidence of spin density waves in $\text{La}_3\text{Ni}_2\text{O}_{7-\delta}$, *Phys. Rev. Lett.* **132**, 256503 (2024).
- [7] Z. Dong, M. Huo, J. Li, J. Li, P. Li, H. Sun, Y. Lu, M. Wang, Y. Wang, and Z. Chen, Visualization of oxygen vacancies and self-doped ligand holes in $\text{La}_3\text{Ni}_2\text{O}_{7-\delta}$, *Nature* **630**, 847 (2024).
- [8] Y. Li, X. Du, Y. Cao, C. Pei, M. Zhang, W. Zhao, K. Zhai, R. Xu, Z. Liu, Z. Li, J. Zhao, G. Li, Y. Qi, H. Guo, Y. Chen, L. Yang, Electronic correlation and pseudogap-like behavior of high-temperature superconductor $\text{La}_3\text{Ni}_2\text{O}_7$, *Chin. Phys. Lett.* **41**, 087402 (2024).
- [9] T. Xie, M. Huo, X. Ni, F. Shen, X. Huang, H. Sun, H. C. Walker, D. Adroja, D. Yu, B. Shen, L. He, K. Cao, and M. Wang, Neutron scattering studies on the high- T_c superconductor $\text{La}_3\text{Ni}_2\text{O}_{7-\delta}$ at ambient pressure, arXiv:2401.12635.
- [10] X. Chen, J. Choi, Z. Jiang, J. Mei, K. Jiang, J. Li, S. Agrestini, M. Garcia-Fernandez, X. Huang, H. Sun, D. Shen, M. Wang, J. Hu, Y. Lu, K.-J. Zhou, and D. Feng, Electronic and magnetic excitations in $\text{La}_3\text{Ni}_2\text{O}_7$, arXiv:2401.12657.
- [11] Z. Dan, Y. Zhou, M. Huo, Y. Wang, L. Nie, M. Wang, T. Wu, and X. Chen, Spin-density-wave transition in double-layer nickelate $\text{La}_3\text{Ni}_2\text{O}_7$, arXiv:2402.03952.
- [12] S. N. Abadi, K. Xu, E. G. Lomeli, P. Pupal, M. Isobe, Y. Zhong, A. V. Fedorov, S. Mo, M. Hashimoto, D. Lu, B. Moritz, B. Keimer, T. P. Devereaux, M. Hepting, and Zhi-Xun Shen, Electronic structure of the alternating monolayer-trilayer phase of $\text{La}_3\text{Ni}_2\text{O}_7$, arXiv:2402.07143.
- [13] Y. D. Li, Y. T. Cao, L. Y. Liu, P. Peng, H. Lin, C. Y. Pei, M. X. Zhang, H. Wu, X. Du, W. X. Zhao, K. Y. Zhai, J. K. Zhao, M.-L. Lin, P. H. Tan, Y. P. Qi, G. Li, H. J. Guo, L. Yang, and L. X. Yang, Ultrafast dynamics of bilayer and trilayer nickelate superconductors, arXiv:2403.05012.
- [14] M. Wang, H.-H. Wen, T. Wu, D.-X. Yao, and T. Xiang, Normal and superconducting properties of $\text{La}_3\text{Ni}_2\text{O}_7$, arXiv:2406.04837.
- [15] Q. Qin and Y.-F. Yang, High- T_c superconductivity by mobilizing local spin singlets and possible route to higher T_c in pressurized $\text{La}_3\text{Ni}_2\text{O}_7$, *Phys. Rev. B* **108**, L140504 (2023).
- [16] Q.-G. Yang, D. Wang, and Q.-H. Wang, Possible s_{\pm} -wave superconductivity in $\text{La}_3\text{Ni}_2\text{O}_7$, *Phys. Rev. B* **108**, L140505 (2023).
- [17] Y.-F. Yang, G.-M. Zhang, and F.-C. Zhang, Interlayer valence bonds and two-component theory for high- T_c superconductivity of $\text{La}_3\text{Ni}_2\text{O}_7$ under pressure, *Phys. Rev. B* **108**, L201108 (2023).
- [18] Y.-B. Liu, J.-W. Mei, F. Ye, W.-Q. Chen, and F. Yang, s^{\pm} -Wave pairing and the destructive role of apical-oxygen

- deficiencies in $\text{La}_3\text{Ni}_2\text{O}_7$ under pressure, Phys. Rev. Lett. **131**, 236002 (2023).
- [19] Y. Shen, M. Qin, and G.-M. Zhang, Effective bilayer model hamiltonian and density-matrix renormalization group study for the high- T_c superconductivity in $\text{La}_3\text{Ni}_2\text{O}_7$ under high pressure, Chin. Phys. Lett. **40**, 127401 (2023).
- [20] Y. Gu, C. Le, Z. Yang, X. Wu, and J. Hu, Effective model and pairing tendency in bilayer Ni-based superconductor $\text{La}_3\text{Ni}_2\text{O}_7$, arXiv:2306.07275.
- [21] Y.-Y. Zheng and W. Wú, Superconductivity in the bilayer two-orbital Hubbard model, arXiv:2312.03605.
- [22] X.-Z. Qu, D.-W. Qu, J. Chen, C. Wu, F. Yang, W. Li, and G. Su, Bilayer t - J - J_\perp model and magnetically mediated pairing in the pressurized nickelate $\text{La}_3\text{Ni}_2\text{O}_7$, Phys. Rev. Lett. **132**, 036502 (2024).
- [23] H. Sakakibara, N. Kitamine, M. Ochi, and K. Kuroki, Possible high T_c superconductivity in $\text{La}_3\text{Ni}_2\text{O}_7$ under high pressure through manifestation of a nearly-half-filled bilayer Hubbard model, Phys. Rev. Lett. **132**, 106002 (2024).
- [24] C. Lu, Z. Pan, F. Yang, and C. Wu, Interlayer coupling driven high-temperature superconductivity in $\text{La}_3\text{Ni}_2\text{O}_7$ under pressure, Phys. Rev. Lett. **132**, 146002 (2024).
- [25] Y.-H. Tian, Y. Chen, J.-M. Wang, R.-Q. He, and Z.-Y. Lu, Correlation effects and concomitant two-orbital s_\pm -wave superconductivity in $\text{La}_3\text{Ni}_2\text{O}_7$ under high pressure, Phys. Rev. B **109**, 165154 (2024).
- [26] J. Chen, F. Yang, and W. Li, Orbital-selective superconductivity in the pressurized bilayer nickelate $\text{La}_3\text{Ni}_2\text{O}_7$: An infinite projected entangled-pair state study, Phys. Rev. B **110**, L041111 (2024).
- [27] Z. Luo, B. Lv, M. Wang, W. Wú, and D.-X. Yao, High T_c superconductivity in $\text{La}_3\text{Ni}_2\text{O}_7$ based on the bilayer two-orbital t - J model, npj Quantum Mater. **9**, 61 (2024).
- [28] J.-R. Xue and F. Wang, Magnetism and superconductivity in the t - J model of $\text{La}_3\text{Ni}_2\text{O}_7$ under multiband gutzwiller approximation, arXiv:2402.07449 (2024).
- [29] J. Wang and Y.-F. Yang, Two-component superconductivity and strange metallicity in $\text{La}_3\text{Ni}_2\text{O}_7$: A Schwinger boson study of the t - V - J model, arXiv:2408.09774.
- [30] Z. Fan, J.-F. Zhang, B. Zhan, D. Lv, X.-Y. Jiang, B. Normand, and T. Xiang, Superconductivity in nickelate and cuprate superconductors with strong bilayer coupling, arXiv:2312.17064.
- [31] K. Jiang, Z. Wang, and F. Zhang, High temperature superconductivity in $\text{La}_3\text{Ni}_2\text{O}_7$, Chin. Phys. Lett. **41**, 017402 (2024).
- [32] R. Jiang, J. Hou, Z. Fan, Z.-J. Lang, and W. Ku, Pressure driven fractionalization of ionic spins results in cuprate-like high- T_c superconductivity in $\text{La}_3\text{Ni}_2\text{O}_7$, Phys. Rev. Lett. **132**, 126503 (2024).
- [33] X.-Z. Qu, D.-W. Qu, W. Li, and G. Su, Roles of Hund's rule and hybridization in the two-orbital model for high- T_c superconductivity in the bilayer nickelate, arXiv:2311.12769.
- [34] Z. Luo, X. Hu, M. Wang, W. Wú, and D.-X. Yao, Bilayer two-orbital model of $\text{La}_3\text{Ni}_2\text{O}_7$ under pressure, Phys. Rev. Lett. **131**, 126001 (2023).
- [35] Y. Cao and Y.-F. Yang, Flat bands promoted by Hund's rule coupling in the candidate double-layer high-temperature superconductor $\text{La}_3\text{Ni}_2\text{O}_7$, Phys. Rev. B **109**, L081105 (2024).
- [36] H. Haug and A.-P. Jauho, *Quantum Kinetics in Transport and Optics of Semiconductors* (Springer-Verlag, Berlin, 1998).
- [37] Y. Meir and N. S. Wingreen, Landauer formula for the current through an interacting electron region, Phys. Rev. Lett. **68**, 2512 (1992).
- [38] Y.-F. Yang and T.-H. Lin, Nonequilibrium transport through a quantum dot weakly coupled to Luttinger liquids, Phys. Rev. B **64**, 233314 (2001).
- [39] Y.-X. Dai and Q.-F. Sun, Andreev reflection in normal metal/charge- $4e$ superconductor junctions, Phys. Rev. B **109**, 144504 (2024).
- [40] Y.-F. Yang, Fano effect in the point-contact spectroscopy of heavy electron materials, Phys. Rev. B **79**, 241107(R) (2009).